

## OUTLIERS FROM THE MAINSTREAM: HOW A MASSIVE STAR CAN PRODUCE A GAMMA-RAY BURST

S. CAMPANA<sup>1</sup>, N. PANAGIA<sup>2,3,4</sup>, D. LAZZATI<sup>5</sup>, A. P. BEARDMORE<sup>6</sup>, G. CUSUMANO<sup>7</sup>, O. GODET<sup>6</sup>, G. CHINCARINI<sup>8,1</sup>, S. COVINO<sup>1</sup>, M. DELLA VALLE<sup>9,10,11</sup>, C. GUIDORZI<sup>8,1</sup>, D. MALESANI<sup>12</sup>, A. MORETTI<sup>1</sup>, R. PERNA<sup>5</sup>, P. ROMANO<sup>8,1</sup>, G. TAGLIAFERRI<sup>1</sup>

*Draft version October 29, 2018*

### ABSTRACT

It is now recognized that long-duration Gamma-Ray Bursts (GRBs) are linked to the collapse of massive stars, based on the association between (low-redshift) GRBs and (type Ic) core-collapse supernovae (SNe). The census of massive stars and GRBs reveals, however, that not all massive stars do produce a GRB. Only  $\sim 1\%$  of core collapse SNe are able to produce a highly relativistic collimated outflow, and hence a GRB. The extra crucial parameter has long been suspected to be metallicity and/or rotation. We find observational evidence strongly supporting that both ingredients are necessary in order to make a GRB out of a core-collapsing star. A detailed study of the absorption pattern in the X-ray spectrum of GRB060218 reveals evidence of material highly enriched in low atomic number metals ejected before the SN/GRB explosion. We find that, within the current scenarios of stellar evolution, only a progenitor star characterized by a fast stellar rotation and sub-solar initial metallicity could produce such a metal enrichment in its close surrounding.

*Subject headings:* gamma rays: bursts — general: gamma-rays, X-rays — individual (GRB 060218)

### 1. INTRODUCTION

The association between long GRBs and SNe hints toward Wolf-Rayet (WR) stars as GRB progenitors (Woosley & Bloom 2006; Fruchter et al. 2006). The WR phase in the evolution of a massive star is relatively short, therefore WR stars are rarely observed. They eject high velocity ( $v_w \sim 1000 - 2000 \text{ km s}^{-1}$ ), mass-loaded winds (mass-loss rates of  $\dot{M} \sim 10^{-5} - 10^{-4} M_{\odot} \text{ yr}^{-1}$ ) as well as massive shells during mass-loss episodes (e.g. Pastorello et al. 2006; Weiler et al. 2007). Signatures for the presence of this material can be expected in the optical light curve of GRB afterglows showing up as flux enhancements in their light curves or as (variable) fine-structure transition lines in their optical spectra. The observations of these features can set important constraints on the density and distance of the absorbing material located either in the star-forming region within which the progenitor formed, or in the circumstellar environment of the progenitor itself (Perna & Loeb 1998; Prochaska et al. 2005).

In the X-ray domain, despite the wealth of features produced by absorption of metals, relatively little progress has

been achieved, mostly due to low statistics and to the relatively poor spectral resolution of the detectors. Here, we consider the Swift (Gehrels et al. 2004) observations of GRB060218. This is the second closest GRB (redshift  $z = 0.033$ ), and the first one showing the shock break out of the SN (Campana et al. 2006). Modelling of the spectra and light curve of the associated SN 2006aj (Pian et al. 2006; Mirabal et al. 2006; Sollerman et al. 2006; Cobb et al. 2006) suggested a progenitor star whose initial mass was  $20 \pm 1 M_{\odot}$  (Mazzali et al. 2006).

This GRB was of very long duration, which allowed Swift to observe it with its narrow field instruments (the X-ray Telescope, XRT, Burrows et al. 2005, and the UV/Optical Telescope, UVOT) during a considerable part of its prompt phase, collecting the largest number of X-ray photons ever. In this letter we exploit the huge number of X-ray photons by analysing the absorption pattern burnt into it by circumburst material.

### 2. X-RAY DATA ANALYSIS

The XRT spectra have been obtained in the Windowed Timing (WT) mode in which a 1D image is obtained by adding the data along the central 200 pixels in a single row (see Hill et al. 2004). The XRT data have been processed using the FTOOLS software package (v. 6.3.1) distributed within HEASOFT. We run the task *xrtpipeline* (v.0.11.4) applying calibration and standard filtering and screening criteria. In particular, we dynamically correct for possible bias offsets computing the bias difference between the on-ground estimated bias median from the last 20 pixels data telemetered with every frame, and the median of the last 20 pixels in the related bias row. Events with grade 0 have been selected in order to attain the best spectral resolution. The XRT analysis has been performed in the 0.3–10 keV energy band (and also in the 0.35–10 keV and 0.25–10 keV energy bands as a consistency check). Given the XRT CCD resolution at low energies ( $\Delta E/E \sim 15\%$ ) we cannot directly see the edges imprint in the X-ray spectrum. Rather we are sensitive to the different slopes in between the edges leading to a precise determination of the depths of the single edges.

We extract the data from an 80 pixel wide region, given the

<sup>1</sup> INAF - Osservatorio Astronomico di Brera, Via Bianchi 46, I-23807 Merate (Lc), Italy

<sup>2</sup> STScI, 3700 San Martin Drive, Baltimore, MD 21218, USA

<sup>3</sup> INAF - Osservatorio Astrofisico di Catania, via S. Sofia 78, I-95123 Catania, Italy

<sup>4</sup> Supernova Ltd., Olde Yard Village 131, Northsound Road, Virgin Gorda, British Virgin Islands

<sup>5</sup> JILA, Campus Box 440, University of Colorado, Boulder, CO 80309-0440, USA

<sup>6</sup> Department of Physics and Astronomy, University of Leicester, University Road, Leicester LE1 7RH, UK

<sup>7</sup> INAF - Istituto di Astrofisica Spaziale e Fisica Cosmica di Palermo, via U. La Malfa 153, I-90146 Palermo, Italy

<sup>8</sup> Università degli studi di Milano Bicocca, piazza delle Scienze 3, I-20126 Milano, Italy

<sup>9</sup> European Southern Observatory, Karl-Schwarzschild-Strasse 2 D-85748 Garching bei München, Germany

<sup>10</sup> INAF - Osservatorio Astronomico di Capodimonte, salita Moiarillo 16, I-80131 Napoli, Italy

<sup>11</sup> International Center for Relativistic Astrophysics Network, Piazza della Repubblica 10, I-65122, Pescara, Italy

<sup>12</sup> Dark Cosmology Centre, Niels Bohr Institute, University of Copenhagen, Juliane Maries vej 30, DK-2100 København Ø, Denmark

strength of the source. The background has been extracted at the edge of the WT slit accounting for only  $\sim 0.5\%$  of the source flux. A dedicated arf file has been generated with the `xrtmkarf` task accounting for bad column holes and correcting for vignetting and point spread function losses. The latest response matrices have been used (v.010, see Campana et al. 2006<sup>13</sup>). These matrices represent a big improvement with respect to the previous version. Calibration data on Mkn421 and isolated neutron stars indicate a good response down to 0.3 keV with no apparent features and data to model ratios always below 10%. A systematic uncertainty of 2.5% has been estimated for very bright sources, at the most.

We divide the entire GRB light curve into two segments taking the XRT peak as dividing line in order to minimize the effects of spectral variations (Campana et al. 2006). This choice results into two intervals: the first 715 s (count rate 72  $\text{c s}^{-1}$ , for a total of 51,000 photons) and the second 1907 s long (73  $\text{c s}^{-1}$ , for a total of 139,000 photons). The peak rate is 130  $\text{c s}^{-1}$ , well below the WT pile-up limit. Data has been rebinned to have at least 100 counts per energy bin.

For the same intervals we extract survey mode BAT data (Barthelmy et al. 2005) in order to fit the XRT and BAT spectra simultaneously and better constrain the XRT high energy part of the emission model. The XRT energy range is 0.3–10 keV and the BAT range is 16–79 keV and 16–37 keV for the first and second (softer) spectrum, respectively.

The large number of counts allowed us for the first time to quantify the abundances of a number of elements, especially those absorbing at low energies. The most prominent absorption edges are those caused by carbon, nitrogen, oxygen, neon, magnesium, silicon, sulfur, iron and nickel (Morrison & McCammon 1983). We considered a simple absorption model including absorption by gas in our Galaxy and intrinsic absorption in the host galaxy (at the known redshift, both modelled with `tbabs`, Wilms et al. 2000, and the standard XSPEC abundance pattern, Anders & Grevesse 1989) folding a black body plus a cut-off power law emission model (the soft component is mandatory to obtain a good fit at variance with most GRBs, Campana et al. 2006). The Galactic absorption has been left free to vary within the interval  $(9.8 - 15) \times 10^{21} \text{ cm}^{-2}$ . This has been estimated by accumulating 360 ks over the field of GRB060218 and fitting the spectra of three relatively bright sources ( $\sim 5 \times 10^{-14} \text{ erg s}^{-1} \text{ cm}^{-2}$ ) with more than 200 counts with the same absorbing column density. The fit of the three sources with a power law is satisfactory and defines the 90% confidence interval as above. This range is also consistent with the column density estimate from HI maps (Dickey & Lockman 1990; Kalberla et al. 2005) and dust NIR maps converted into X-ray absorption (Schlegel et al. 1998). The intrinsic column density is free to vary at the host galaxy redshift of  $z = 0.03342$  (Wiersema et al. 2007). We also considered the inclusion of a gain fit (a small rigid adjustment of the energy scale due to residuals in the bias subtraction) and a systematic uncertainty at the 2.5% level.

Adopting a solar metallicity for the host galaxy absorption provides a rather poor fit with large residuals in the 0.4–0.6 keV energy range, as expected (see Fig. 1). We then left free the metallicity of the host galaxy. We obtained a better fit with a lower metallicity (using the `tbvarbas` model)  $Z = 0.20_{-0.06}^{+0.02} Z_{\odot}$  (hereon uncertainties are given

at the 90% confidence level) and a large column density of  $N_{\text{HI}} = (2.0_{-0.4}^{+0.7}) \times 10^{22} \text{ cm}^{-2}$ . The metallicity is higher than the mean value determined for the host galaxy ( $Z = 0.07_{-0.02}^{+0.06} Z_{\odot}$ , see Wiersema et al. 2007). In addition, the (solar composition) HI column density is so high that, even with that low metallicity, it would imply an extinction of a factor of  $\gtrsim 50$  higher than what has been inferred from the strengths of the sodium absorption lines in the host galaxy ( $E(B - V) = 0.042 \pm 0.003$ , Wiersema et al. 2007) or from the Balmer decrement ( $E(B - V) \lesssim 0.03$ , Guenther et al. 2006). The improvement from a solar metallicity absorber to a free metallicity absorber is at the  $4.2 \sigma$  level (by means of an F-test). A similar discrepancy between optical and X-ray absorption is frequently observed in GRB afterglows (Galama & Wijers 2001; Stratta et al. 2005; Watson et al. 2007) even adopting the dust to gas ratio of the Small Magellanic Cloud (SMC, Pei et al. 1992).

Despite the large number of counts, we do not have enough sensitivity to leave free the abundances of all individual elements in the fitting procedure. We focus therefore on the CNO abundances (with absorption edges at rest-frame energies of 0.28, 0.41 and 0.54 keV, respectively) as additional free parameters, while we adopt the abundances derived from optical studies for the remaining elements. The CNO abundances are (much) larger than the solar value. Fitting for a gain offset further improves the fit with values in the  $-30$  to  $-10$  eV range. With this model we obtain a better fit to the data with an F-test probability of 5.1–5.5  $\sigma$  (depending on the adopted systematic uncertainties in the response matrix). The host galaxy column density is in this case  $N_{\text{HI}} = 1.1_{-0.4}^{+0.9} \times 10^{21} \text{ cm}^{-2}$ , which is consistent with the optical absorption measured in the host galaxy for an SMC dust to gas ratio. This result may indicate that the discrepancy between optical and X-ray absorption is simply due to a large amount of circumburst material enriched in CNO elements. If these are mostly in the form of gas then they cause absorption in the X-rays but not in the optical.

The error on the CNO abundances has been evaluated with the `steppar` command within XSPEC to circumvent non-monotonicity in  $\chi^2$  space. We also tried a different absorption model using `varabs` within XSPEC, obtaining very similar results.

An additional issue could be the rapidly evolving spectrum, leading to spurious spectral features. To test whether this could pose a problem, we divide the two initial spectra into six smaller intervals each. We generate the appropriate response and then fit with the same model as above (and absorption parameters fixed) the resulting spectra. Then, we simulate spectra with a factor of 10 more photons and join them. The two resulting fake spectra recover quite well the initial absorption pattern (now left free to vary) within the fitting uncertainties.

GRB060218 occurred in February 2006. Data has been processed with the appropriate version 6 gain files (`swxwtgains0_20010101v006.fits`, calibrated in 2005). As a test, we also used version 7 of the gain file (`swxwtgains0_20010101v007.fits`, calibrated in late 2006–2007). This new gain file together with a new arf file (yet unreleased) provides a superior description of the spectral models but it is fully appropriate for observations taking place nowadays. We reprocess all the data and fit them with the same best fit model. We check that also in this case we obtain the same results well within the uncertainties and, more importantly, the same ratios by number. This positive test further strengthens our observational result.

<sup>13</sup> <http://heasarc.gsfc.nasa.gov/docs/heasarc/caldb/swift/docs/xrt/SWIFT-XRT-CALDB-09>

## 3. DISCUSSION AND CONCLUSIONS

Since we do not have a knowledge of the total mass involved, the most insightful measurement we obtain from X-ray best fit data is the ratio by number of the abundances of C, N and O. We derive  $C/N = 0.9^{+3.2}_{-0.7}$  and  $O/N = 0.3^{+0.6}_{-0.2}$  (or logarithmic abundances relative to the solar value  $[C/N] = -0.5^{+0.7}_{-1.5}$  and  $[O/N] = -1.4^{+0.5}_{-0.2}$ ). This extremely low ratio O/N is very difficult to account for in terms of standard interstellar medium and of stellar evolution models of isolated stars. In particular, solar metallicity models are unable to reproduce these abundance ratios (Hirschi et al. 2005; Portinari et al. 1998). Possibly, binary evolutionary models can account for this constraints more easily, having more degrees of freedom, but recent models seem to indicate that conditions similar to single star progenitors are needed (Detmers et al. 2008).

A key ingredient in the evolution of single massive stars is missing: rotation-induced mixing in the stellar interior. If the ejected mass reflects the C/N and O/N ratios that would be expected at the end of the main sequence phase as observed in several nebulae around bright stars, we would need a large rotation-induced mixing fraction with only  $\sim 10\%$  of the initial mass unprocessed (based on calculations in Lamers et al. 2001). This mixing can occur only in the case of a very fast stellar rotation (close to break-up). A viable alternative could be also provided by a close binary system, either in terms of tidal locking or evolution through a common envelope phase during which an enriched shell might be ejected.

The collapsar scenario requires massive helium stars with rapidly rotating cores to produce a GRB (Woosley 1993). However, stellar models with magnetic torques fail to retain such high core angular momentum. In the last few years there has been mounting theoretical support the idea that only massive stars that are initially very rapidly rotating and have sufficiently low metallicities can satisfy the conditions for GRB formation (Yoon & Langer 2005; Woosley & Heger 2006). In fact, below a suitable metallicity threshold, a rotationally-induced mixing process produces a quasi chemically homogeneous stellar evolution avoiding the spin-down of the stellar core. As a test-bed we consider massive star evolution models at sub-solar initial metallicities (Yoon et al. 2006). We also limit the mass range of the progenitor to  $15 - 25 M_{\odot}$ , according to the detailed modelling of the supernova ejecta (Mazzali et al. 2006). We find that a number of models are able to satisfy our constraints (see Fig. 2). All these models are characterized by a fast semi-convective mixing of the core. Within the initial mass range of the progenitor we are able to constrain the initial fraction of the Keplerian velocity ( $v_K$ ) of the equatorial rotational velocity to  $0.45 \lesssim v_{\text{ini}}/v_K \lesssim 0.8$  and the initial metallicity to  $Z < 0.1 Z_{\odot}$ . With these parameters the progenitor star fits nicely within the allowed region for the GRB production (Yoon et al. 2006). It thus appears that the observations of GRB060218 provide the first observational evidence that only a progenitor star characterized by a fast stellar rotation and sub-solar initial metallicity can lead to such an explosive event.

We acknowledge S.-C. Yoon for help with Fig. 2 and D.N. Burrows for comments. SC thanks Dr. G. Balza, E. Biguzzi, M. Tavola for making this letter possible. We acknowledge partial support from ASI (ASI/I/R/039/04) and PPARC. The Dark Cosmology Centre is supported by the Danish National

TABLE 1  
SPECTRAL FITTING RESULTS WITH DIFFERENT ENERGY RANGES AND FIT OPTIONS.

Model	Energy range (keV)	Gain	System. (2.5%)	$\chi^2_{\text{red}}$ (dof) <sup>+</sup> [nhp <sup>+</sup> %]	F-test* ( $\sigma$ )
1#	0.25–10	N	N	1.11 (830) [0.01]	–
2#	0.30–10	N	N	1.10 (827) [0.02]	–
3#	0.35–10	N	N	1.10 (825) [0.02]	–
4	0.3–10	Y	N	1.07 (825) [0.06]	5.5
5	0.3–10	Y	Y	0.96 (825) [81.]	5.1

<sup>+</sup> dof: degrees of freedom; nhp: null hypothesis probability.

\* Improvement in the fit by leaving free to vary the abundances of CNO, evaluated by means of an F-test.

# The enlargement of the energy band produces a worsening of the  $\chi^2$ , indicating that the low energy part of the considered interval plays an important role in the evaluation of the goodness of fit.

Research Foundation.

TABLE 2  
SPECTRAL FIT ABSORPTION PARAMETERS.

Element	Edge energy (keV)	Edge energy rest-frame (keV)	Solar abundance table (H= 1)	Abundance ( $Z_{\odot}$ )	Column density ( $\text{cm}^{-2}$ )
C	0.268	0.277	$3.6 \times 10^{-4}$	$15_{-10}^{+48}$	$6_{-4}^{+19} \times 10^{18}$
N	0.380	0.392	$1.1 \times 10^{-4}$	$52.5_{-12}^{+28}$	$7_{-2}^{+4} \times 10^{18}$
O	0.508	0.525	$8.3 \times 10^{-4}$	$2.2_{-0.2}^{+0.3}$	$2_{-0.3}^{+0.2} \times 10^{18}$

## REFERENCES

- Anders, E., Grevesse, N. 1989, *Geochimica et Cosmochimica Acta*, 53, 197
- Barthelmy, S.D., et al. 2005, *Sp. Sci. Review*, 120, 143
- Burrows, D.N., et al. 2005, *Sp. Sci. Review*, 120, 165
- Campana, S., et al. 2006, *Nat*, 442, 1008
- Cobb, B.E., et al. 2006, *ApJ*, 645, L113
- Detmers, R.G., et al. 2008, *A&A* in press (astro-ph/0804.0014)
- Dickey, J.M., Lockman, F.J. 1990, *ARA&A*, 28, 215
- Fruchter, A.S., et al. 2006, *Nat*, 441, 463
- Galama, T.J., Wijers, R.A.M.J. 2001, *ApJ*, 594, L209
- Gehrels, N., et al. 2004, *ApJ*, 611, 1005
- Guenther, E.W., et al. 2006, *GCN* 4863
- Hill, J.E., et al. 2004, *SPIE*, 5165, 217
- Hirschi, R., Meynet, G., Maeder, A. 2005, *A&A*, 259, 629
- Kalberla, P.M.W., et al. 2005, *A&A*, 440, 775
- Lamers, H.J.G.L.M., et al. 2001, *ApJ*, 551, 764
- MacFadyen, A.I., Woosley, S.E. 1999, *ApJ*, 524, 262
- Mazzali, P.A., et al. 2006, *Nat*, 442, 1018
- Mirabal, N., et al. 2006, *ApJ*, 643, L99
- Morrison, R., McCammon, D. 1983, *ApJ*, 270, 119
- Pastorello, A., et al. 2007, *Nat*, 447, 829
- Pei, Y.C. 1992, *ApJ*, 395, 130
- Perna, R., Loeb, A. 1998, *ApJ*, 509, L85
- Pian, E., et al. 2006, *Nat*, 442, 1011
- Portinari, L., Chiosi, C., Bressan, A. 1998, *A&A*, 334, 505
- Prochaska, J.X., Chen, H.-W., Bloom, J.S. 2005, *ApJ*, 648, 95
- Schlegel D.J., Finkbeiner, D.P., Davis, M. 1998, *ApJ*, 500, 525
- Sollerman, J., et al. 2006, *A&A*, 454, 503
- Stratta, G., et al. 2005, *A&A*, 441, 83
- Watson, D., et al., 2007, *ApJ*, 660, L101
- Weiler, K. W., et al. 2007, *ApJ*, 671, 1959
- Wiersema, K., et al. 2007, *ApJ*, 464, 529
- Wilms, J., Allen, A., McCray, R. 2000, *ApJ*, 542, 914
- Woosley, S.E. 1993, *ApJ*, 405, 273
- Woosley, S.E., Bloom, J.S. 2006, *ARA&A*, 44, 507
- Woosley, S.E., Heger, A. 2006, *ApJ*, 637, 914
- Yoon, S.-C., Langer, N. 2005, *A&A*, 443, 643
- Yoon, S.-C., Langer, N., Norman, C. 2006, *A&A*, 460, 199

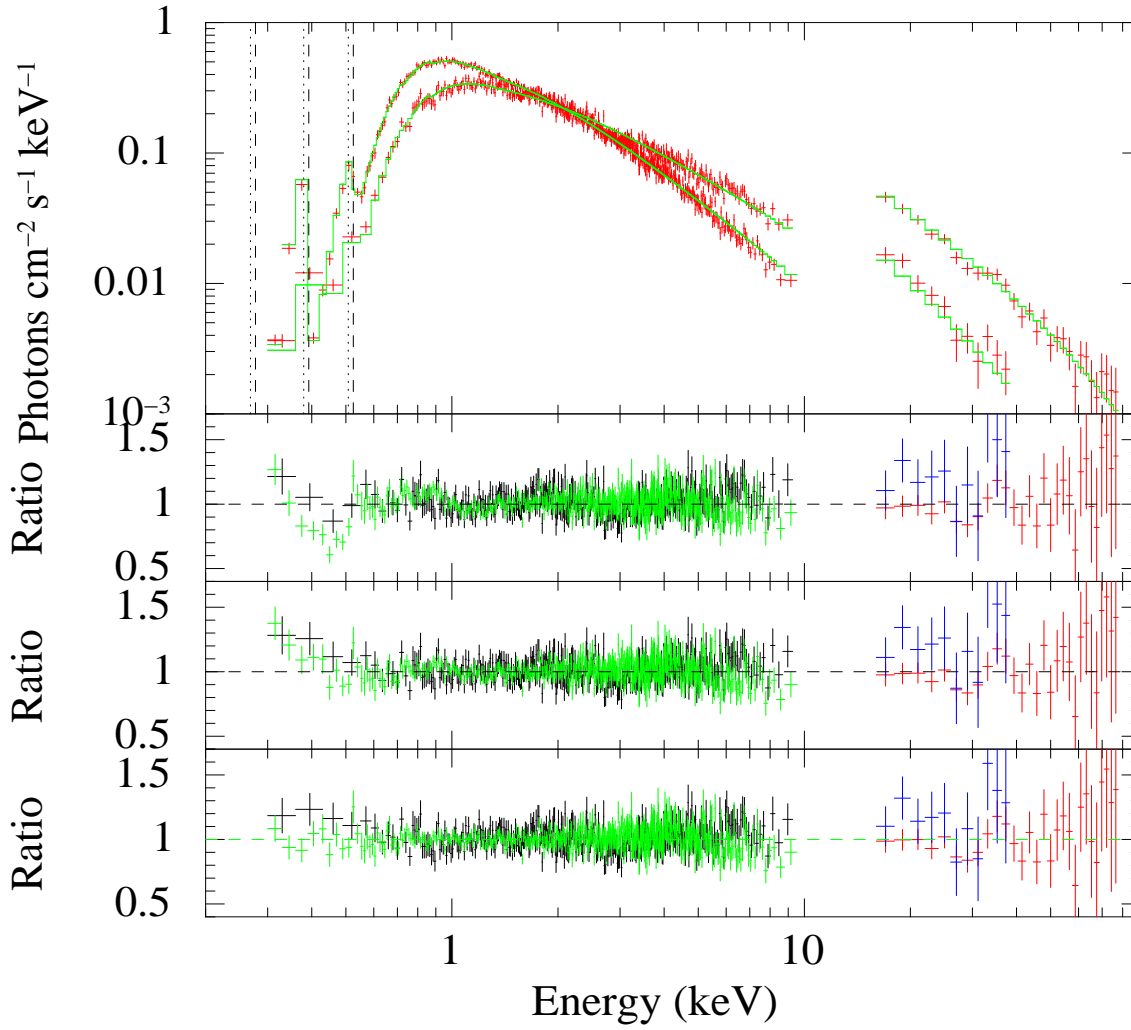


FIG. 1.— The upper panel shows the XRT and BAT unfolded energy spectra for the two time intervals discussed in the text. Dashed and dotted lines indicate the rest-frame and redshifted edge energy of the CNO, respectively. The three lowest panels show the spectral residuals as ratio between the data and the following spectral model. For the second panel we considered a solar metallicity absorber in the host galaxy. For the third panel we let the metallicity of the host galaxy absorption free to vary (keeping the standard solar abundance pattern fixed). For the lowest panel we fixed the the metallicity to the one derived from optical studies at  $0.07 Z_{\odot}$  of the entire host galaxy and leave free only the CNO abundances (for both absorbing models we use the `tbvarbas` model).

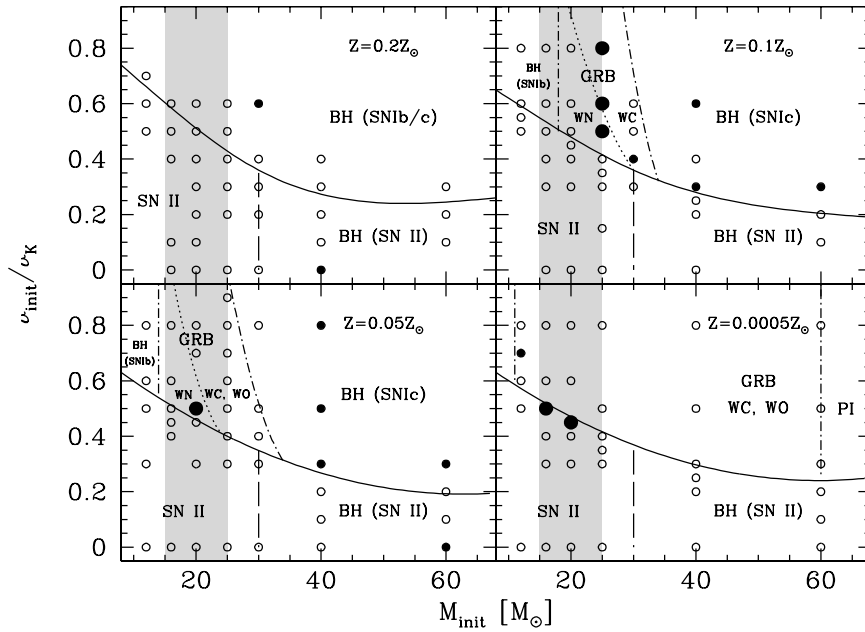


FIG. 2.— Constraints from the abundance ratio in the plane of initial mass and initial stellar velocity (in units of equatorial Keplerian velocity) as described in Yoon et al. (2006). The four panels refer to four different initial metallicities ( $0.2, 0.1, 0.05, 0.0005 Z_{\odot}$  clockwise). We note that the mean host galaxy metallicity has been estimated in  $Z \sim 0.07 Z_{\odot}$ . Different final end-products can be identified in this plane for rotating single massive stars. The solid line divides the plane into two parts, where stars evolve quasi-chemically homogeneous above the line, while they evolve into the classical core-envelope structure below the line. The dotted-dashed lines bracket the region of quasi-homogeneous evolution where the core mass, core spin and stellar radius are compatible with the collapsar model for GRB production (absent at  $Z = 0.2 Z_{\odot}$ ). The GRB production region is divided into two parts, where GRB progenitors are WN or WC/WO types. The dashed line in the region of non-homogeneous evolution separates Type II supernovae (SN II; left) and black hole (BH; right) formation, where the minimum mass for BH formation is simply assumed to be  $30 M_{\odot}$ . We added to these planes single star models allowed by the abundance constraints derived from X-ray data; open circles represent instead models not satisfying these constraints. Larger dots refer to models within the  $15 - 25 M_{\odot}$  (initial) progenitor mass range (i.e. within the vertical strip), based the mass estimate from Mazzali et al. (2006).